

Phase-Induced Amplitude Apodization of Telescope Pupils for Extrasolar Terrestrial Planet Imaging

Olivier Guyon

Subaru Telescope, National Astronomical Observatory of Japan, 650 North A'ohoku Place, Hilo, HI 96720 USA

the date of receipt and acceptance should be inserted later

Abstract. In this paper, an alternative to the classical pupil apodization techniques (use of an amplitude pupil mask) is proposed. It is shown that an apodized pupil suitable for imaging of Extrasolar planets can be obtained by reflection of an unapodized flat wavefront on 2 mirrors. By carefully choosing the shape of these 2 mirrors, it is possible to obtain a contrast better than 10^9 at a distance smaller than $2\lambda/d$ from the optical axis. Because this technique preserves both the angular resolution and light gathering capabilities of the unapodized pupil, it allows efficient detection of terrestrial extrasolar planets with a 1.5m telescope in the visible.

Key words. Techniques: high angular resolution, (Stars:) planetary systems, Telescopes

1. Introduction

With more than 100 exoplanets now known, direct imaging of extrasolar terrestrial planets (ETPs) is of great scientific importance. Unlike indirect detection techniques, such as radial velocity, astrometry or transit observations, it can allow a spectral decomposition of the light reflected (in the visible) or emitted (in the infrared) by the planet. Such a spectral analysis is essential to study the habitability of ETPs.

Unfortunately, the large contrast (about 10^9 in visible, and 10^6 in thermal infrared) between ETPs and their parent star, along with the small separation ($0.1''$ for a Earth-Sun system at 10pc) makes direct detection very challenging. Ground-based telescopes of reasonable size (less than 100m diameter) cannot image ETPs in the visible because of the strong wavefront errors due to atmospheric turbulence, and ground-based thermal infrared observations lack the required sensitivity.

Two solutions are seriously considered to image ETPs from space :

- An optical telescope with a high-performance coronagraphic device.
- A thermal infrared ($10\mu\text{m}$) nulling interferometer (Leger et al., 1996, Angel & Woolf, 1997, Guyon & Roddier, 2002, Riaud et al., 2002).

With an optical telescope, the use of a high-performance coronagraphic device is essential to suppress, or strongly reduce, the amplitude of the “wings” of the Point-Spread Function (PSF). Without such a device, the light from the ETPs is “lost” in the strong wings of the central star image.

One such coronagraphic technique, “classical” pupil apodization (CPA), aims at modifying the pupil transmission function by placing an amplitude mask in the pupil plane to reduce the amplitude of the PSF wings. This adaptation of the pupil to the problem of high-contrast imaging can allow the PSF wings to be reduced to 10^{-10} of the central surface brightness at a distance of a few λ/d . Many pupil apodization masks have been proposed for this purpose (Jacquinot & Roizen-Dossier, 1964, Nisenson & Papaliolios, 2001, Aime et al., 2001, Spergel, 2001, Kuchner & Traub, 2002), and optimization techniques to generate these masks have been developed (Gonsalves & Nisenson, 2002). Unfortunately, this technique reduces the flux sensitivity (a large fraction of the light is absorbed by the apodization mask) and the angular resolution (the transmission at the edges of the apodized pupil is lower than at the center) of the telescope. Moreover, in many CPA designs, only part of the field of view is suitable for planet detection.

In this paper, an alternative to the CPA technique is proposed: phase-induced amplitude apodization (PIAA). Instead of producing the apodized pupil by using an amplitude mask in the pupil plane, the pupil is modified by reflection on 2 mirrors (which can be the primary and secondary mirrors of the telescope) whose phase aberrations are chosen to produce an exit pupil which greatly reduces intensity the PSF wings.

The PIAA technique is first briefly presented in §2. In §3, the properties of the images obtained by this technique are studied, and several solutions are presented to use a PIAA telescope as a wide field coronagraphic imager. In §4, the performance of the PIAA technique for ETPs detection is studied.

2. Description of the technique

2.1. Overview

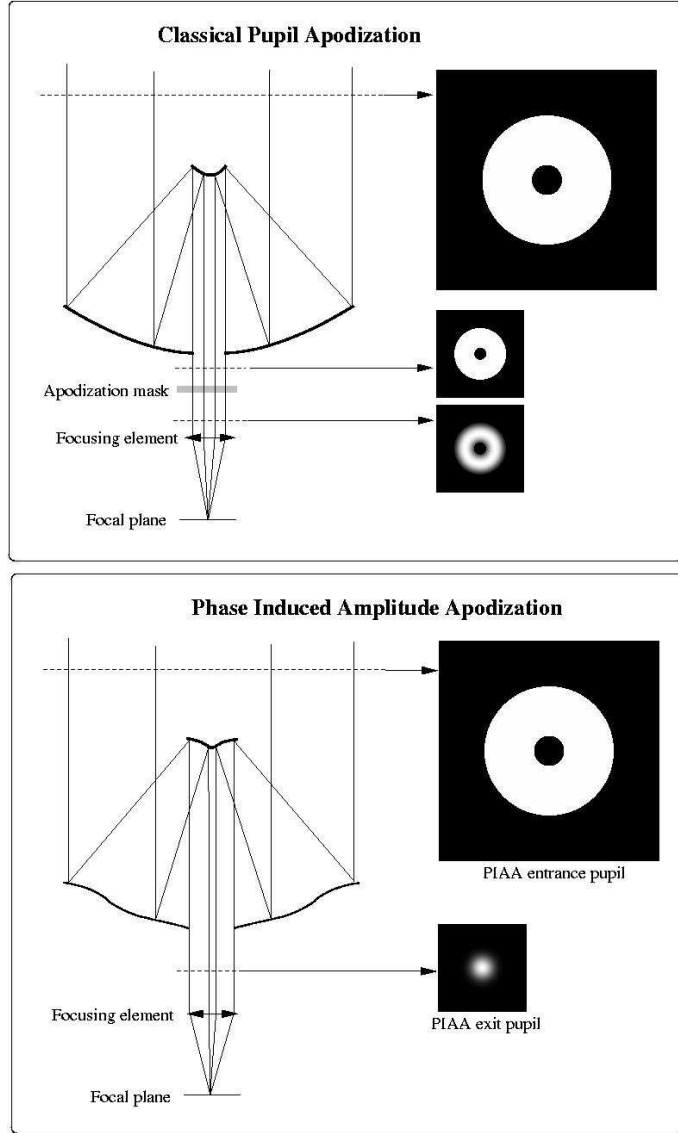


Fig. 1. Schematic representation of the Classical Pupil Apodization (CPA) technique (top) and the Phase Induced Amplitude Apodization (PIAA) technique (bottom).

The general principle of the Phase Induced Amplitude Apodization (PIAA) technique is illustrated in figure 1. In a classical telescope, the shape and distribution of light intensity across the pupil is preserved by the reflective optical elements, and only a focus phase term is introduced to form the image on the detector. For clarity, in Figure 1, this focus phase term is represented by a separate optical element, and consequently, the primary and secondary mirrors' sole function is to reduce the physical size of the beam. To obtain an "apodized" pupil with a telescope, a transmissive mask can be placed in a pupil plane (where the wavefronts are flat) as shown in Figure 1. The PIAA technique uses phase aberrations in two mirrors to produce an apodized pupil. In Figure 1, the PIAA technique is

shown with the primary and secondary mirrors of the telescope used to generate the desired apodized pupil. Two reflections are needed to transform the PIAA entrance pupil into the PIAA exit pupil, which has simultaneously the desired light amplitude distribution and a flat wavefront (aberration-free).

In the PIAA optical design represented in figure 1, the role of the primary mirror is mainly to modify the light distribution across the pupil, while the secondary mirror is used mostly to correct the phase aberrations introduced by the primary mirror. These two separate functions are in reality somewhat shared between the two optical elements. As shown on Figure 1, the PIAA technique can be used to remove the central obstruction from the pupil.

2.2. Computing the mirror shapes

2.2.1. Circular-symmetric pupils

In this section, a geometric method is given to compute the shape of the two mirrors needed to transform any given circular symmetric entrance pupil into the desired circular symmetric exit pupil. Both pupils are free from phase aberrations and are entirely characterized by their radial light distributions, $f_1(r)$ and $f_2(r)$ respectively. The total light flux F is conserved in the PIAA :

$$\int_0^{R_1} r f_1(r) dr = \int_0^{R_2} r f_2(r) dr = F \tag{1}$$

with R_1 and R_2 the radius of the primary and secondary mirrors respectively.

The first step of the geometric construction is to establish a correspondence between the radius in the entrance pupil and the radius in the exit pupil: for a light ray entering the entrance pupil at a radius r_1 , what is the radius r_2 at which this light ray is exiting the exit pupil ?. This problem is solved by measuring the total flux of the entrance pupil enclosed inside the radius r_1 , and choosing r_2 such that this flux equals the total flux of the exit pupil enclosed inside r_2 :

$$\int_0^{r_1} r f_1(r) dr = \int_0^{r_2} r f_2(r) dr = t \times F \tag{2}$$

where $0 < t < 1$ is the fraction of the light enclosed inside the radii considered. A large number of radii $r_{1i}, i = 0 \dots N - 1$, of increasing values, are chosen to sample the entrance pupil, and the corresponding radii r_{2i} are computed for the exit pupil. The entrance pupil and exit pupil light rays can then be drawn (see figure 2). The path of the the first light ray can be drawn because the position of the points at which this ray hits the primary and secondary mirrors are known from the distance between the 2 mirrors. For each mirror, the angle of incidence of this first light ray with the surface of the mirror is measured (it is half of the angle between the incoming and reflected light rays). This angle of incidence gives the slope of the mirror surface at the reflection point, and a small mirror segment can then be constructed up to the point where the next light ray is encountered. This process is repeated until the last light ray, and leads to an approximation of the mirrors shape made of N straight segments. By increasing the number of sampling

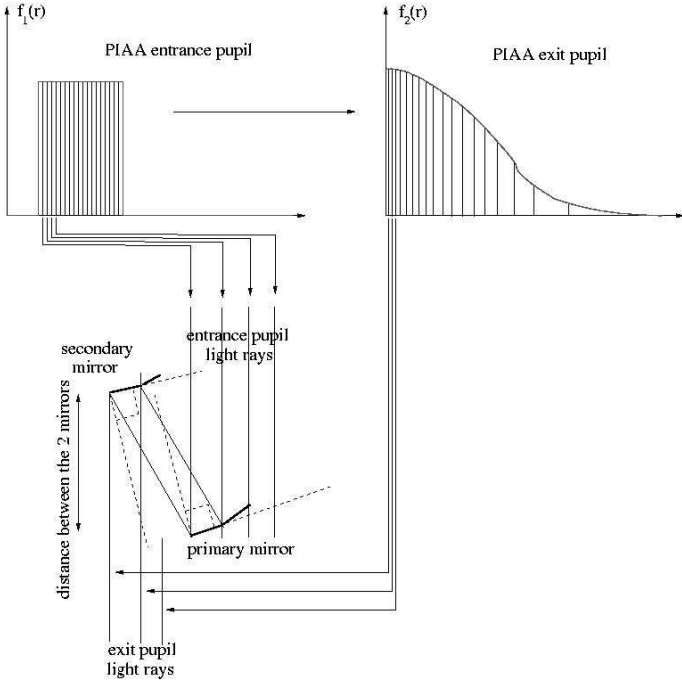


Fig. 2. A method for geometric construction of the PIAA primary and secondary mirror shapes for circular-symmetric pupils.

rays N , the obtained mirror shapes $M_1(r)$ (primary mirror) and $M_2(r)$ (secondary mirror), by construction, satisfy the following conditions :

- Both the incoming (entrance pupil) and outgoing (exit pupil) light rays are parallel to each other, and, therefore, the incoming and outgoing wavefronts are flat (a direct consequence of Huygens-Fresnel principle).
- The reflexions of the incoming light rays on M_1 and then M_2 produce the desired exit pupil light distribution $f_2(r)$.

Software was written to compute $M_1(r)$ and $M_2(r)$ from $f_1(r)$ and $f_2(r)$, and, to check the validity of the obtained solution, the optical pathlength difference OPD_i between rays i and 0 was computed for $i = 1 \dots N - 1$. It was found that the residual OPD errors decrease toward 0 when N increases:

$$\lim_{N \rightarrow \infty} \left(\sum_{i=1}^{N-1} (OPD_i)^2 \right) = 0. \quad (3)$$

If $f_2(r) = \alpha^2 \times f_1(\alpha \times r)$ (the exit pupil is identical to the entrance pupil, scaled by a factor α), then the software correctly produces a primary mirror M_1 which is a parabola.

This geometric construction is equivalent to solving the following differential equation:

$$\frac{d M_1(r_1(t))}{d r_1(t)} = \frac{d M_2(r_2(t))}{d r_2(t)} = \frac{\sqrt{A(t)^2 + B(t)^2} - B(t)}{A(t)} \quad (4)$$

where

$$A(t) = r_2(t) - r_1(t), \quad (5)$$

$$B(t) = M_2(r_2(t)) - M_1(r_1(t)), \quad (6)$$

and $r_1(t)$ and $r_2(t)$ are respectively the radii in the entrance and exit pupils inside which the fraction of the total flux is t (equation 2). The initial conditions are the size of the central obstruction ($r_1(0)$), if any, and the distance between the primary and secondary mirror ($M_2(0)$), assuming that $M_1(0) = 0$). The first equality in equation (4) is ensuring that the PIAA exit wavefront is flat: for a given light ray (parameter t), the angles of the 2 reflections are opposite and produce an output light ray parallel to the incoming light ray.

2.2.2. Off-axis telescopes with circular symmetric entrance and exit pupils.

High dynamical range imaging, whether with the CPA or PIAA techniques, is easier without the central obstruction and the “shadow” of the structure that supports the secondary mirror (spider). Although the PIAA technique can “erase” the central obstruction (as illustrated in figure 1), a large central obstruction produces a greater mismatch between $f_1(r)$ and $f_2(r)$ which, as will be shown later, reduces the imaging field of view. Moreover, removing the spider with the PIAA technique can be difficult.

Just as in the case of “classical” telescopes, the mirror shapes computed by the technique presented above can be modified to be used in an off-axis telescope by simply adding a constant slope across the mirror. In the case of a classical telescope, this operation transforms a parabola into an off-axis parabola ($x^2 + \alpha \times x = (x + \alpha/2)^2 - \alpha^2$), and it can be applied on both the primary and secondary mirrors. It is easy to check that this operation only “steers” the whole beam, but does not introduce phase aberrations or modifies the light amplitude distribution in planes perpendicular to the central light ray.

2.3. One example

In this section, the PIAA technique is illustrated by an example. The desired radial light intensity $f_2(r)$ to be obtained by the PIAA technique is shown in fig. 3, along with the radial profile of the PSF it produces. The function f_2 was computed through the iterative algorithm presented in §4.1, and is optimized to reduce the intensity of the PSF at distances greater than λ/d . The strict constraints put on the PSF produced a function f_2 which is null on 3 intervals separated by intervals in which f_2 is strictly positive. Very good apodization functions which have no such null intervals exist, and are also suitable for ETPs detections.

Figure 4 shows two possible optical configurations: on-axis telescope or off-axis telescope. In both cases the distance between the 2 mirrors is less than the diameter of the primary, and the primary is therefore close to a fast parabola ($F/D < 1$). In this configuration, the primary mirror is quite close to a parabola, as shown in figure 4, lower left: for a 2m diameter primary mirror, the difference between the primary mirror and a perfect parabola is less than 1 mm. This deviation from a perfect parabola is mostly seen in the outer edge of the primary, where the surface is “bent” to reflect a small amount of the light into the outer part of the secondary (the “wings” of the f_2 function). The shape of the secondary mirror is also pecu-

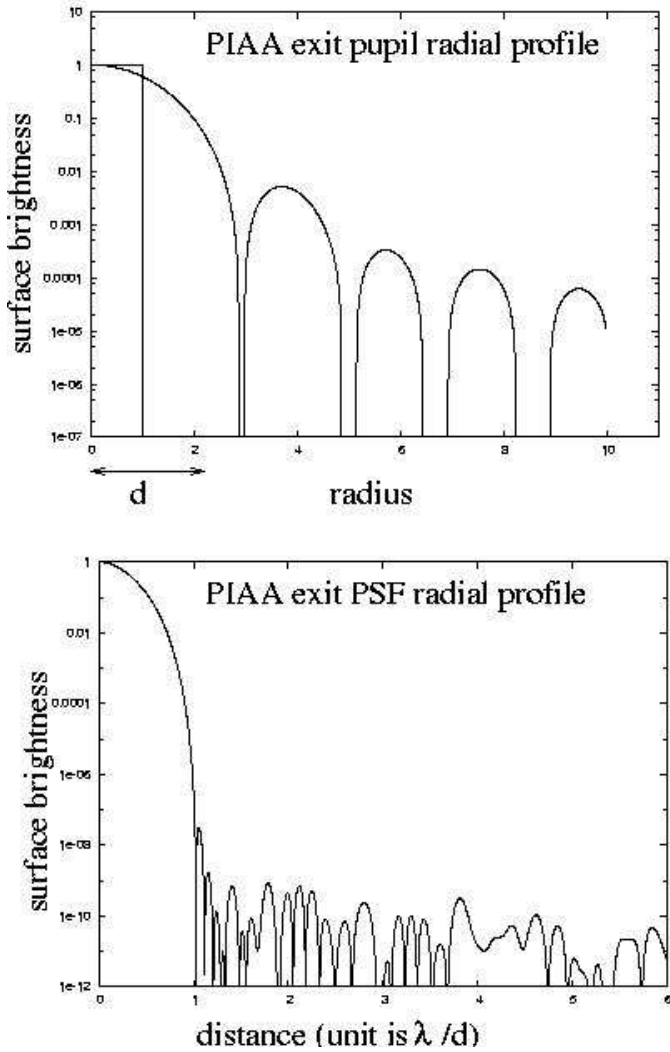


Fig. 3. Radial profile $f_2(r)$ of the PIAA exit pupil (left) and radial profile of the corresponding PSF (right) for the example considered. The radial profile of the unapodized pupil of equal total flux is shown as a dashed line, and its diameter d is used to measure the distances in the PSF (unit is λ/d).

liar, and its central part is approximated by a cone (the slope of the mirror does not tend to 0 at small distance from the optical axis) in the case of a telescope with central obstruction.

3. Field of view and possible use as a coronagraph

3.1. Field of view of the technique

In a classical telescope, an off-axis source produces the same wavefront as an on-axis source modulo a phase slope. This slope is given by the position of the source relative to the optical axis. As a result, the image of an off-axis source is obtained by translation of the image of an on-axis source.

The PIAA technique redistributes the complex amplitude of the light in the entrance pupil to form the PIAA exit pupil. The incoming wavefront of an on-axis point source is flat and its phase is constant across the pupil, and because the PIAA does not introduce phase aberration, this property is still true in the

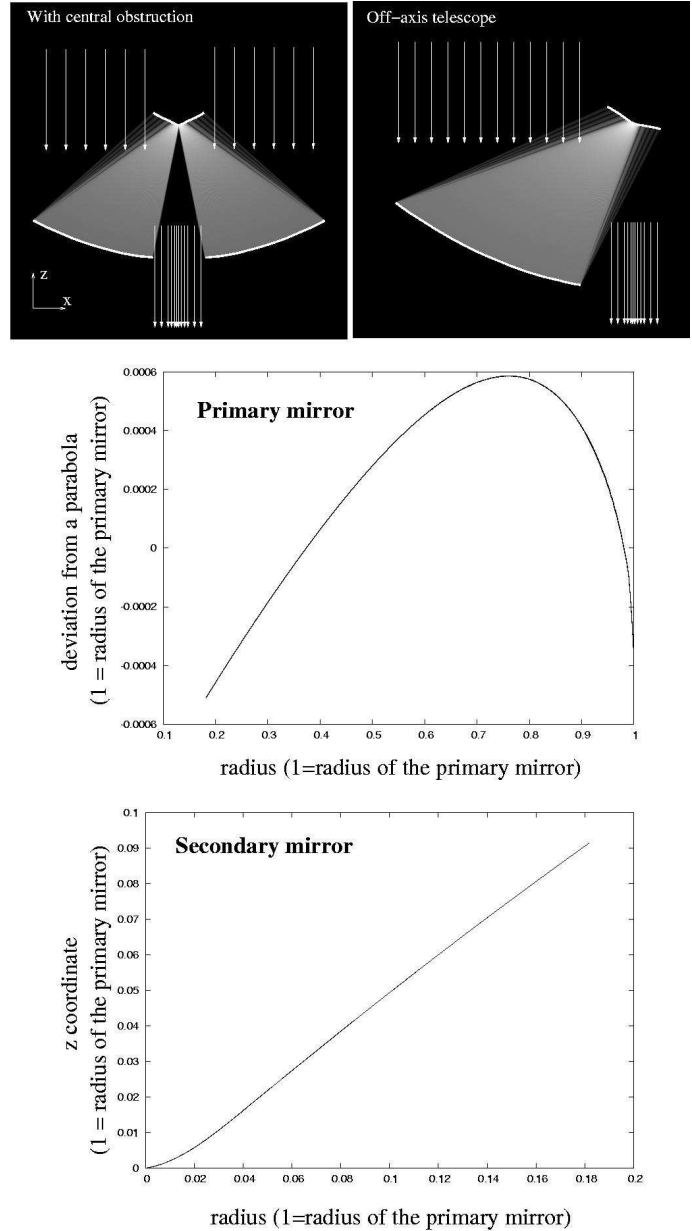


Fig. 4. Optical designs for the PIAA example studied: telescope with central obstruction (upper left) and off-axis telescope (upper right). Both images show a cut of the mirror shapes and the density of light rays between the 2 reflexions. A few light rays are represented entering the telescopes and the corresponding light rays exiting the telescope are shown. The shape of the optics is shown for the telescope with central obstruction: deviation of the primary mirror to a parabolic fit (center) and shape of the secondary mirror (bottom).

PIAA exit pupil. However, the geometric redistribution of light between the entrance pupil and the exit pupil of the PIAA does not preserve the constant phase slope of a wavefront from an off-axis source. The PSF is therefore not translation-invariant as shown in figure 5: the PSF becomes less concentrated for off-axis sources.

This effect does not affect the performance of a PIAA imager for detection of ETPs within a few times λ/d because the

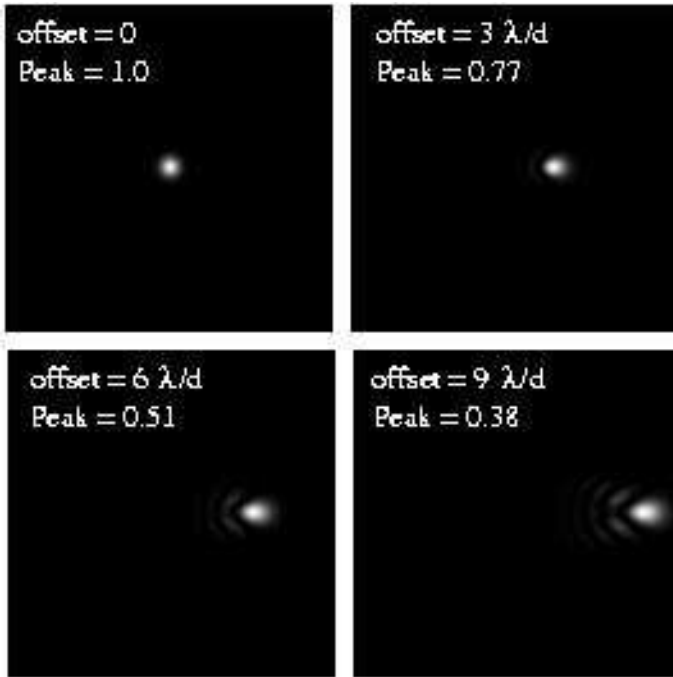


Fig. 5. Degradation of the PSF quality with distance to the optical axis for the example studied in §2.3. The brightness scale is linear and identical for all images.

loss of PSF quality is moderate to small in this central region, and the image of the star (defined by the PSF of an on-axis source) remains very contrasted (contrast better than 10^9 at $2 \times \lambda/d$ in the example considered). However, wide-field imaging performance of the PIAA imager are seriously affected by this effect. In the particular example studied, the point source detection limit for planets at large angular separation would be affected, especially in the presence of a strong background (exozodiacal light for example).

3.2. Extending the field of view of the PIAA imager

The first solution to the field of view problem is to carefully choose the light distribution of the PIAA exit pupil to maintain a bright, sharp and contrasted PSF core even at large angular separations from the optical axis. This can be done by imposing additional constraints in the iterative algorithm used to compute $f_2(r)$ (see section §4.1), in order to minimize the mismatch between $f_1(r)$ and $f_2(r)$. In particular, if the entrance pupil of the PIAA is an unobstructed disk, as much as possible of the light in the PIAA exit pupil should be within a large “flat” central part of $f_2(r)$: this “flat” part will produce a bright and sharp diffraction core while the wings of f_2 will be used to cancel the diffraction and yield a very contrasted on-axis PSF.

A hybrid CPA/PIAA optical configuration is also possible. For example, the central part of the f_2 function can be obtained by classical apodization while the wings of the f_2 function are obtained by the PIAA technique. This hybrid configuration would extend the field of view at the expense of a loss of light.

3.3. Use as a coronagraph

The PIAA entrance pupil (telescope pupil) offers a wide field of view but a low contrast PSF, while the PIAA exit pupil offers a good contrast PSF but a small field of view. It is possible to combine the advantages of these two pupils by using the PSF obtained by the PIAA exit pupil (apodized) to mask the central source and then restore the original pupil (telescope pupil) before forming the final image. Figure 6 illustrates this optical configuration.

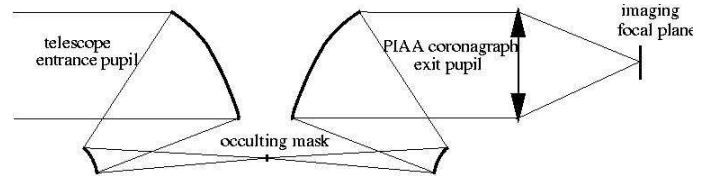


Fig. 6. Schematic representation of the PIAA coronagraph.

If the occulting mask is removed, the effect of the 4 mirrors cancel each other and the PIAA coronagraph exit pupil is identical to the telescope entrance pupil. The PSF is therefore translation-invariant and of good quality across a wide field of view. An off-axis source is not affected by the occulting mask because its image misses the small mask in the first focal plane, but the central source’s light is blocked by the occulting mask, whose size is chosen to match the size of the on-axis PSF.

The optical quality requirements are much more strict for the two mirrors before the mask than after the mask: the PSF wings must be kept very faint at the first focal plane. Therefore, the addition of 2 extra optical elements to build a PIAA coronagraph does not pose serious difficulties, and the wavefront accuracy for these 2 mirrors can be as low as $\lambda/10$ without significant loss of performance.

This technique is very similar to the coronagraphic technique used in the interferometer concept studied by Guyon & Roddier (2002), where pupil densification is used to first adapt the interferometer’s sparse pupil to a coronagraph, and pupil redilution is then used to restore the entrance’s pupil shape. This later step is essential to restore the wide field of view that is lost in the pupil densification process.

4. Performance

4.1. Choice of the apodization function

The performance of the PIAA imager/coronagraph is solely a function of f_2 , the light distribution in the PIAA exit pupil. The constraints on the choice of f_2 are first discussed :

- **(1) Positivity of f_2 .** In the technique presented in this paper, there is no convenient way to introduce an achromatic π phase shift in parts of the pupil, and f_2 is therefore real and positive.
- **(2) Contrast of the on-axis PSF.** The main requirement for the detection of ETPs is to obtain a PSF which offers high contrast (typically 10^9 to 10^{10}) at small angular distances (one to two times λ/d).

- **(3) Finite size of the secondary mirror.** The finite size of the secondary mirror and the fact that the “core” of the PIAA exit pupil cannot be made arbitrarily small (because of Fresnel diffraction) imposes a limit of the extent of f_2 .
- **(4) Field of view considerations.** This constraint has been shown in §3, and requires a f_2 function which is somewhat flat in its central part (small values of r). The PIAA coronagraph does not have this constraint.

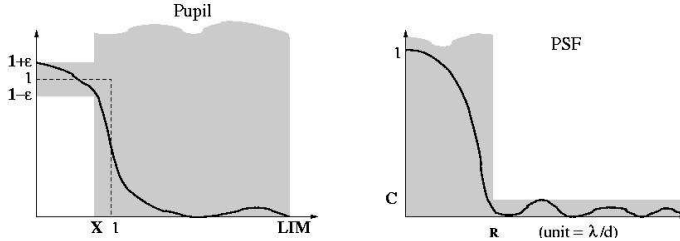


Fig. 7. Constraints imposed on the function f_2 and on the on-axis PSF. The grey area represents the permitted values for both $f_2(r)$ and the PSF radial profile and the thick curves represent examples of permitted functions. In the pupil radial profile, the dashed line represents the unapodized unobstructed pupil of diameter d , and of total flux equal to the total flux of the PIAA exit pupil.

Figure 7 shows how these constraints were applied with 5 parameters:

- ϵ : maximum deviation of f_2 from the flat reference pupil.
- X : radius of the PIAA exit pupil inside which the maximum deviation of f_2 from the flat reference pupil is enforced.
- LIM : maximum size of the PIAA exit pupil.
- C : contrast to be achieved by the PSF.
- R : radial distance outside of which the contrast to be achieved by the PSF is enforced.

These constraints are used in a Gerchberg-Saxton (Gechberg & Saxton, 1972) type iterative algorithm to find a function f_2 which satisfies all constraints. At each iteration, the Fourier transform of the pupil (the focal plane light complex amplitude) is first computed, and the PSF constraints (2) are used to modify the focal plane light complex amplitude. Another Fourier transform is performed to compute the pupil light complex amplitude distribution, which, in turn, is modified by the constraints (1), (3) and (4). After several iterations, convergence of the pupil light complex amplitude distribution toward a suitable function f_2 usually occurs. If no convergence occurs, the constraints parameters are relaxed (for example, larger size of the secondary mirror, or lower required contrast of the PSF) until convergence occurs. Because this study is limited to radially symmetric pupils, all computations are actually done in one dimension.

The example shown in section §2.3 was obtained by this algorithm with a set of parameters which yields a PSF suitable for ETPs detection in the imager configuration ($\epsilon = 0.25$, $X = 0.8$, $LIM = 10$, $C = 10^{-9}$, $R = 1.0$). Although the field of view of this particular example is well suited for ETPs detection with

a small telescope ($d \approx 2m$), wide-field coronagraphic imaging would require either a different choice of values for ϵ and X , or a coronagraphic configuration.

4.2. Performances and comparison with classical apodized pupils

Classical apodization techniques (CPA) have several disadvantages compared to the PIAA technique:

- **Loss of flux.** The transmission of classical apodization masks is usually between 0.1 and 0.5, while no light is absorbed with the PIAA.
- **Loss of angular resolution.** In CPAs, the apodization mask usually has a lower transmission at the edges of the pupil, resulting in a loss of angular resolution by a factor of approximately 2. This loss of resolution requires the use of a larger telescope and also results in lower sensitivity, since more background light (from scattering of the central source’s light or emission from the zodiacal/exozodiacal clouds) is mixed with the companion’s PSF.
- **Limited useful field of view.** Most apodization masks produce a PSF in which only a fraction of the field is usable for ETPs detection.

When choosing a apodization mask, CPAs technique must find an acceptable tradeoff between these 3 different losses, and minimization of one these losses usually comes at the expenses of another loss.

To estimate the performance of the PIAA and CPAs techniques for direct planet imaging, detection Signal to Noise Ratio (SNR) is computed for a representative case, with the diameter of the telescope as the main variable. Four configurations were tested under the same conditions :

- **PIAA configuration.** The example studied in §2.3 was adopted.
- **Jacquinot configuration** (Jacquinot & Roizen-Dossier, 1964). The pupil transmission is equal to 1 if and only if:

$$|y| < R \times \left(e^{-\left(\frac{\alpha x}{R}\right)^2} - e^{-\alpha^2} \right) \quad (7)$$

with R the radius of the pupil and $\alpha = 2$, and it is equal to 0 everywhere else.

- **Spergel configuration** (Spergel, 2001). The pupil transmission is equal to 1 if and only if:

$$y_0(x) < |y| < y_0(x) + y_w(x) \quad (8)$$

with

$$y_w(x) = R \times \left(e^{-\left(\frac{\alpha x}{R}\right)^2} - e^{-\alpha^2} \right) \quad (9)$$

and

$$\int_{y_0(x)}^{y_0(x)+y_w(x)} y^2 dy = \beta y_w(x) \quad (10)$$

with $\alpha = 2$ and $\beta = 0.4 \times R^2$, and it is equal to 0 everywhere else.

- **Apodized Square Aperture (ASA) configuration** (Nisenson & Papaliolios, 2001). The pupil transmission is 0 everywhere except in a square of radius R , inside which it is equal to:

$$P(x, y) = \left(1 - \left(\frac{x}{R}\right)^\nu\right) \times \left(1 - \left(\frac{y}{R}\right)^\nu\right) \quad (11)$$

with R the square radius and $\nu = 5$.

The 3 CPA pupils adopted for the comparison are shown in fig. 8, as well as the corresponding PSFs.

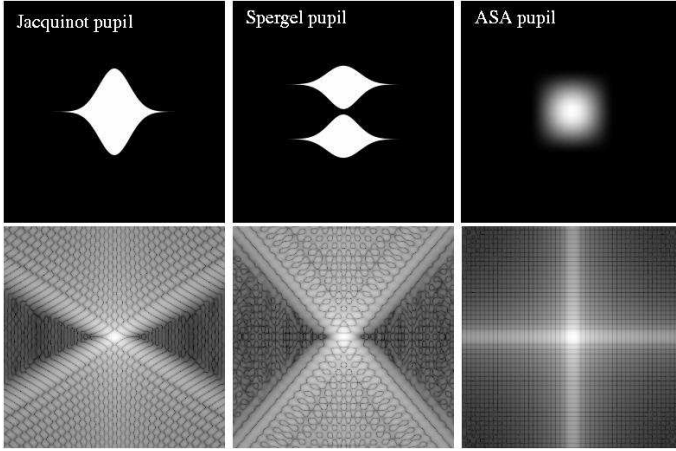


Fig. 8. CPA pupils adopted for the comparison between PIAA and CPA techniques performances. The pupils are shown on the upper row and the corresponding PSFs are shown in the lower row (logarithmic scaling).

To compute the SNR of a companion detection, only photon noise is considered, and the noiseless PSF is supposed to be perfectly known. For a given image of the star/planet system, the best detection SNR is obtained by computing the optimally weighed sum of the PSF-subtracted image pixel values. The weight of each pixel in the sum is proportional to the square of the SNR on that pixel and the resulting detection SNR is

$$SNR = \sqrt{\int_{x,y} \left(\frac{I_c(x,y)}{\sqrt{I_c(x,y) + I_s(x,y)}} \right)^2 dx dy} \quad (12)$$

where $I_c(x, y)$ is the image of the companion and $I_s(x, y)$ is the image of the central star. In the case of the PIAA configuration, the PSF is not translation-invariant, and has to be computed both for the central star and the planet. For a given optical configuration, this SNR is function of the contrast between the star and the companion, their angular separation, the luminosity of the star and the diameter of the telescope. For PSFs which are not rotational-symmetric, the SNR is also a function of the position angle (PA), in which case the detection SNR can be written

$$SNR = \int_{PA=0}^{2\pi} \sqrt{SNR(PA)} dPA \quad (13)$$

where $SNR(PA)$ is computed by equation 10. For the Jacquinot and Spergel pupils, where the PSF contrast is very good only

for a range of PA values, this equation is equivalent to rejecting the “unusable” regions of the PSF (too low SNR).

The 4 optical configurations are tested on a $m_v = 5$ star with a planet 10^9 times fainter at a separation of $0.1''$. The central wavelength is $0.5\mu m$ and the spectral bandwidth is $0.2\mu m$. No zodiacal or exozodiacal light was included in this simple simulation, and the detectors are supposed to be perfect (no readout noise).

The results of the performance analysis is shown in fig 9. The 3 CPA configurations require telescopes of diameters be-

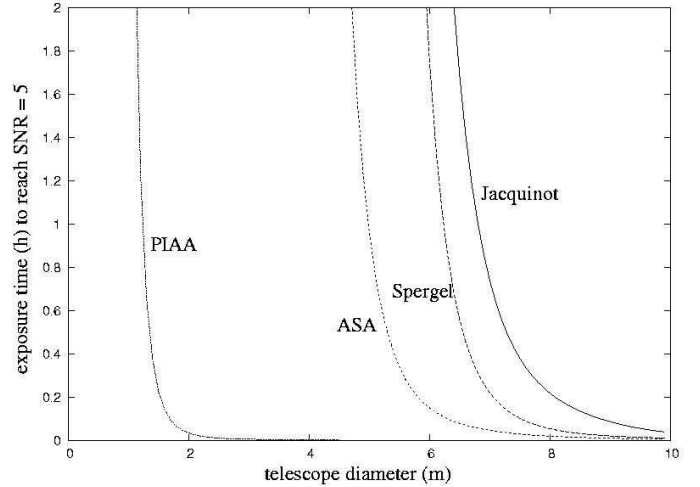


Fig. 9. Telescope diameter needed to detect (SNR=5) a companion $0.1''$ from a $m_v = 5$ star with a flux ratio of 10^9 . The central wavelength is $0.5\mu m$ and the bandwidth is $0.2\mu m$.

tween 5 and 7 meters to detect (SNR=5) the ETP in one hour exposure time, while the PIAA configuration reaches the same performance with a 1.5m diameter telescope. This result is explained by careful analysis of the table 1.

	Transmission	IWD	Discovery Space
PIAA	1.00	$\approx 1.5\lambda/d$	1.00
Jacquinot	0.285	$\approx 5\lambda/d$	≈ 0.25
Spergel	0.273	$\approx 4\lambda/d$	≈ 0.5
ASA	0.107	$\approx 4\lambda/d$	≈ 0.5 (increases with distance)

Table 1. Main properties of the PIAA configuration and 3 CPA configurations. IWD stands for Inner Working Distance, and is the smallest angular distance at which a 10^9 contrast is reached in the PSF. The Discovery space is the fraction of the field of view usable for faint companion detection.

The Inner Working Distance (IWD), which is the angular separation at which the contrast of the PSF reaches 10^9 , is about 3 times larger for the CPAs than for the PIAA configuration. This means that, in the visible, the minimum telescope diameter required to detect ETPs in reasonable exposure times is about 4 to 5 meters for CPA configurations while it is only 1.5

meter for the PIAA configuration. In addition, the low transmission and small discovery space of the CPA configuration yield a comparatively lower efficiency compared to the PIAA configuration. The product of the transmission by the discovery space is a good approximation of this efficiency: for the CPA configurations, this efficiency is about 0.1 (responsible for an increase of the exposure time by a factor of 10).

The fact that ETPs can be detected with a 1.5m telescope is not surprising when the number of incoming photons is considered. In the typical example studied above, the ETP photon flux is about $0.2 \text{ ph.s}^{-1}.\text{m}^{-2}$, and about 1200 photons can be collected by a 1.5m telescope in 1 hour.

5. Conclusion

The PIAA technique makes it possible to image ETPs with a telescope smaller than 2m in less than 1h exposure time, which makes it a very attractive alternative to classical pupil apodization (CPA) techniques. A direct comparison between the 2 techniques shows that a factor of 3 in telescope diameter can be gained by using the PIAA configuration.

The PIAA technique can also be used to adapt the telescope's pupil to a coronagraph. For example, it can produce a pupil suitable for the phase mask coronagraph (Roddier & Roddier, 1997), which can only reach full coronagraphic extinction with a suitable apodized pupil (Guyon & Roddier, 2000, Aime et al., 2002, Guyon & Roddier, 2002, Soummer et al., 2003). This pupil adaptation to the coronagraph can also be performed on the densified pupil of an interferometer. Another interesting application is to increase the coupling efficiency between a telescope and a single mode fiber in interferometers. By producing a suitable unobstructed apodized exit pupil, the PIAA technique can increase the coupling efficiency by 22% for an unobstructed telescope pupil, and by 93% for the CFHT pupil (0.44 central obstruction).

Although no detailed simulation of the sensitivity of the PIAA technique to wavefront errors was made in this study, the wavefront tolerance is probably similar to what it is for CPA techniques. A wavefront distortion of $\lambda/1000$ is sufficient to already compromise ETPs detection because of the phase errors in the PIAA exit pupil. This relatively small wavefront error would however not produce significant modifications of the distribution of the light in the PIAA exit pupil. A analogy with classical telescopes can be drawn: the effect of phase-induced amplitude variations in the pupil of classical telescopes are negligible when compared to the effect of phase errors.

The polishing of the PIAA imager/coronagraph optics could however be difficult, especially at the edge of the primary mirror, but the moderate mirror size needed to detect ETPs, on the other hand, makes polishing easier than polishing of mirrors 3 to 4 times larger for CPA imagers.

The PIAA technique could be also used on a smaller size telescope (about 0.5m to 1m diameter), or at a longer wavelength, to detect Jupiter-like planets. The technique could also replace Lyot coronagraphs on ground-based telescopes with adaptive optics for scientific projects requiring lower contrast ratios. The PIAA technique could be implemented with 2 small

high-order deformable mirrors on "classical" telescopes, and these 2 mirrors could simultaneously correct the wavefront aberrations of the telescope's optics and reduce the intensity of the PSF diffraction wings.

Acknowledgements. The author is thankful to Thomas Kane for suggestions to improve the manuscript, and to Lyu Abe and Koji Murakawa for discussions about this idea.

References

- Aime, C., Soummer, R., Ferrari, A. 2001, *A&A*, 379, 697.
- Aime, C., Soummer, R., Ferrari, A. 2002, *A&A*, 389, 334.
- Angel, J.R.P., Woolf, N.J. 1997, *ApJ*, 475, 373.
- Gerchberg, R.W., Saxton, W.O. 1972, *Optik*, 35, 237.
- Gonsalves, R., Nisenson, P. 2002, preprint, (astro-ph/0210166)
- Guyon, O., Roddier, F. 2002, *Proc. of the conf. "Darwin and Astronomy - The infrared Space Interferometer"*, Stockholm, Sweden, 17-19 November 1999, 41.
- Guyon, O., Roddier, F. 2002, *A&A*, 391, 379.
- Jacquinet, P., Roizen-Dossier, B. 1964, *Prog. Optics*, 3, 29.
- Kuchner, M.J., Traub, W.A. 2002, *ApJ*, 570, 900.
- Leger, A., Mariotti, J-M., Mennesson, B., Ollivier, M., Puget, J. L., Rouan, D., Schneider, J. 1996, *Icarus*, 123, 249.
- Nisenson, P., Papaliolios, C. 2001 *ApJ*, 548, L201.
- Riaud, P., Boccaletti, A., Gillet, S., Schneider, J., Labeyrie, A., Arnold, L., Baudrand, J., Lardire, O., Dejonghe, J., Borkowski, V. 2002, *A&A*, 396, 345.
- Roddier, F., Roddier, C. 1997, *PASP*, 109, 815.
- Soummer, R., Aime, C., Falloon, P.E 2003, *A&A*, 397, 1161.
- Spergel, D.N. 2001, preprint (astro-ph/0101142).